




Cite this: *RSC Adv.*, 2018, 8, 41439

# Efficient photoelectrochemical water oxidation using a TiO<sub>2</sub> nanosphere-decorated BiVO<sub>4</sub> heterojunction photoanode †

Wenchao Jiang, Yi Jiang, \* Jing Tong, Qian Zhang, Siyuan Li, Haili Tong and Lixin Xia \*

Constructing heterojunctions by coupling dissimilar semiconductors is a promising approach to boost charge separation and charge transfer in photoelectrochemical (PEC) water splitting. In this work, we fabricated a highly efficient TiO<sub>2</sub>/BiVO<sub>4</sub> heterojunction photoanode for PEC water oxidation *via* a simple hydrothermal method. The resulting heterojunction photoanodes show enhanced PEC performance compared to the bare BiVO<sub>4</sub> due to the simultaneous improvements in charge separation and charge transfer. Under simulated sunlight illumination (AM 1.5G, 100 mW cm<sup>-2</sup>), a high photocurrent of 3.3 mA cm<sup>-2</sup> was obtained at 1.23 V (vs. the reversible hydrogen electrode (RHE)) in a neutral solution, which exceeds those attained by the previously reported TiO<sub>2</sub>/BiVO<sub>4</sub> heterojunctions. When a molecular Co-cubane catalyst was immobilized onto the electrode, the performance of the TiO<sub>2</sub>/BiVO<sub>4</sub> heterojunction photoanode can be further improved, achieving a higher photocurrent density of 4.6 mA cm<sup>-2</sup> at 1.23 V, an almost three-fold enhancement over that of the bare BiVO<sub>4</sub>. These results engender a promising route to designing an efficient photoelectrode for PEC water splitting.

Received 2nd November 2018  
Accepted 3rd December 2018

DOI: 10.1039/c8ra09072f

rsc.li/rsc-advances

## Introduction

With gradual, increasing consumption resulting in the depletion of traditional fossil fuels, new forms of energy are being investigated. Sunlight has attracted more interest as it is the most abundant renewable energy source.<sup>1–3</sup> Solar energy, a new type of renewable energy, has the advantages of being a clean and inexhaustible source of energy and is attracting research interest. Splitting water into hydrogen and oxygen using sunlight, *via* photoelectrochemical (PEC) devices, is a promising method of converting and storing solar energy as a chemical fuel.<sup>2–5</sup> To date, an enormous effort has been invested in this field, however, the development of a highly efficient PEC water splitting cell for solar-to-hydrogen fuel conversion remains a challenge.<sup>6,7</sup> And the PEC water splitting using semiconductors has received increasing attention, owing to the semiconductors have excellent light absorption characteristics, for example, bismuth vanadate (BiVO<sub>4</sub>) and TiO<sub>2</sub>. BiVO<sub>4</sub> has appropriate band-edge position (2.4 eV) and a wide range of absorption of sunlight.<sup>8,9</sup> However, the unmodified BiVO<sub>4</sub> has significant electron–hole recombination and poor water oxidation kinetics.<sup>10</sup> Various strategies have been implemented to address these restrictions, such as nanostructured

control,<sup>11</sup> elemental doping,<sup>12,13</sup> loading cocatalysts such as Co-Pi,<sup>14–16</sup> FeOOH<sup>17</sup> and NiOOH,<sup>10,18</sup> construction of heterojunction,<sup>19,20</sup> and plasmonic enhancement.<sup>21–23</sup>

In principle, constructing heterojunctions is the most effective and direct way to promote the efficiency of charge-separation in photoelectrodes. Many studies have investigated BiVO<sub>4</sub>-based heterojunction photoanodes, such as WO<sub>3</sub>/BiVO<sub>4</sub>,<sup>24–26</sup> TiO<sub>2</sub>/BiVO<sub>4</sub>,<sup>27–29</sup> *etc.* These composites have been demonstrated to have higher PEC performance compared to BiVO<sub>4</sub>. TiO<sub>2</sub> has been intensively studied as a candidate photoanode due to its favourable band-edge positions, high resistance to photocorrosion, physical and chemical stability, nontoxicity and low cost.<sup>30,31</sup> Recent studies have reported an improvement in PEC water oxidation using TiO<sub>2</sub>/BiVO<sub>4</sub> heterojunctions.<sup>32</sup> However, a high photocurrent density for this heterojunction electrode is scarce.

In this study, a facile hydrothermal method using modified nanoporous BiVO<sub>4</sub> photoanodes with TiO<sub>2</sub> nanospheres was proposed to develop TiO<sub>2</sub>/BiVO<sub>4</sub> heterojunction photoanodes. The BiVO<sub>4</sub> layers in this photoanode absorb sunlight and the TiO<sub>2</sub> nanospheres facilitate the separation and transmission of the photogenerated charge in BiVO<sub>4</sub>. The shift of TiO<sub>2</sub> and BiVO<sub>4</sub> interfacial Fermi levels result in the formation of an n–n junction at the interface,<sup>33</sup> promoting electron–hole separation. The proposed TiO<sub>2</sub>/BiVO<sub>4</sub> heterojunction photoanodes had good PEC performance. A high photocurrent density of 3.3 mA cm<sup>-2</sup> was achieved at 1.23 V, compared to a reversible hydrogen electrode (RHE) in a neutral electrolyte, which is much higher

College of Chemistry, Liaoning University, Shenyang 110036, Liaoning, China. E-mail: jiangyi@lnu.edu.cn; lixinia@lnu.edu.cn

† Electronic supplementary information (ESI) available. See DOI: 10.1039/c8ra09072f



than that of BiVO<sub>4</sub> and exceeds other TiO<sub>2</sub>/BiVO<sub>4</sub> heterojunctions reported. To further optimise the kinetics of surface water oxidation of photoanodes, a molecular Co-cubane water oxidation catalyst (WOC) was immobilized on the electrode and an extremely high photocurrent density of 4.6 mA cm<sup>-2</sup> was achieved at 1.23 V vs. RHE.

## Experimental section

### Fabricate of the BiVO<sub>4</sub> photoanode

The BiVO<sub>4</sub> electrodes were prepared by using an electrodeposition process as reported.<sup>10</sup> Briefly, the electrodeposited solution was prepared as follow: 2.91 g Bi(NO<sub>3</sub>)<sub>3</sub>·5H<sub>2</sub>O (99.0%, AR) and 9.96 g KI (99.0%, AR) were dissolved in 150 mL deionized water respectively before its pH was adjusted to 1.7 by adding HNO<sub>3</sub>, then this solution was mixed with 20 mL of absolute ethanol contained 1.49 g *p*-benzoquinone (99%) by stirring for a few minutes vigorously. A three-electrode cell was used for electrodeposition, with an FTO as the working electrode, an Ag/AgCl (3.5 M KCl) reference, and a platinum counter electrode. A CHI660 was used for electrodeposition studies. Deposition was carried out potentiostatically at -0.1 V vs. Ag/AgCl for 3 min at 30 °C (equivalent to passing a total charge of 0.45C cm<sup>-2</sup>). All prepared films were rinsed by deionised water and blow-dried with nitrogen. 10 mL of a dimethyl sulfoxide (DMSO, AR) solution containing 1.06 g vanadyl acetylacetonate (VO(acac)<sub>2</sub> 98%) was placed on the BiOI electrode. Then the BiOI electrodes were annealed at 450 °C (ramping rate = 2 °C min<sup>-1</sup>) for 2 h. After annealing, the as deposited film was converted to crystalline BiVO<sub>4</sub> and amorphous V<sub>2</sub>O<sub>5</sub>, and pure BiVO<sub>4</sub> was obtained by dissolving the V<sub>2</sub>O<sub>5</sub> in 1 M NaOH under stirring for several minutes.

### Fabricate of the TiO<sub>2</sub>/BiVO<sub>4</sub> photoanode

The TiO<sub>2</sub>/BiVO<sub>4</sub> electrode was developed using a hydrothermal method. The TiO<sub>2</sub> nanospheres were formed using a hydrolysis reaction. 1 mL of TiCl<sub>4</sub> solution was added to 50 mL deionized water, and centrifuged for 5 min at 10 000 rpm until the suspended precipitate was spun down into a pellet. The supernatant was removed and precipitate resuspended in deionized water. The TiO<sub>2</sub> aqueous solution was subjected to ultrasonic treatment to promote the dispersion of TiO<sub>2</sub> nanospheres throughout the solution. A BiVO<sub>4</sub> electrode was immersed into the TiO<sub>2</sub> aqueous solution for 10 min (10 min-TiO<sub>2</sub>/BiVO<sub>4</sub>), 30 min (30 min-TiO<sub>2</sub>/BiVO<sub>4</sub>) and 60 min (60 min-TiO<sub>2</sub>/BiVO<sub>4</sub>) at 60 °C. Finally, the electrode was washed using deionized water and then calcined at 500 °C for 2 h in air (2 °C min<sup>-1</sup>).

### Development of a TiO<sub>2</sub> photoanode

A TiO<sub>2</sub> electrode was prepared using a spin-coating method. TiO<sub>2</sub> was deposited onto the FTO using spin coating at 1000 rpm for 20 s. The spin coating solution was the previously described solution in Section 2. After spin coating, the samples were annealed at 500 °C for 2 h with a temperature increase of 2 °C min<sup>-1</sup>.

### Synthesis of Co-cubane catalyst

The Co-catalyst was synthesised as below: Co(NO<sub>3</sub>)<sub>2</sub>·6H<sub>2</sub>O (2.90 g, 10 mmol) and CH<sub>3</sub>COONa·3H<sub>2</sub>O (2.70 g, 20 mmol) added in 30 mL methanol and heated to refluxing temperature, then 4-cyanopyridine (10 mmol) was added to the reaction mixture. 30% hydrogen peroxide (5 mL) was slowly added into the reaction mixture, which was held at reflux for a further 4 h. The reaction mixture was cooled and concentrated in a rotary evaporator, and the aqueous layer was separated by adding CH<sub>2</sub>Cl<sub>2</sub>. The light pink aqueous layer was discarded, and the CH<sub>2</sub>Cl<sub>2</sub> layer was dried using anhydrous Na<sub>2</sub>SO<sub>4</sub>. An olive-green compound precipitated out on addition of petroleum ether. Fig S1† is the structure of the Co-cubane. Fig S2† is the <sup>1</sup>H-NMR of the catalyst. <sup>1</sup>H-NMR (500 MHz, CD<sub>3</sub>OD): 8.65 (d, 8H), 7.62 (d, 8H), 2.2 (d, 12H).

### Preparation of the Co-cubane/TiO<sub>2</sub>/BiVO<sub>4</sub> photoanode

The catalyst solution is prepared by dissolving the Co-cubane catalyst into solution (CH<sub>3</sub>OH/CH<sub>2</sub>Cl<sub>2</sub>/Nafion mixture (7 : 2.5 : 0.5, v/v)) at a concentration of 1 mM. A 10 μL of the cobalt catalyst was then cast onto the surface of the TiO<sub>2</sub>/BiVO<sub>4</sub> electrode and dried at room temperature.

### Photoelectrochemical measurements

The PEC performance of the BiVO<sub>4</sub> and TiO<sub>2</sub>/BiVO<sub>4</sub> electrodes were tested in 0.1 M PBS solution and AM 1.5 G simulated sunlight illumination (100 mW cm<sup>-2</sup>). The active surface area of the BiVO<sub>4</sub> and TiO<sub>2</sub>/BiVO<sub>4</sub> heterojunctions were 1 cm<sup>2</sup>. A CHI660 was used for electrochemical PEC measurements which contained samples as the working electrode, an Ag/AgCl (3.5 M KCl) reference and a platinum counter electrode. EIS measurements was carried out at 0.6 V versus Ag/AgCl. Mott-Schottky measurements were performed under dark conditions, in the potential range -0.6 to +1.0 V versus Ag/AgCl with 500 Hz. All the potentials are presented against the reversible hydrogen electrode (RHE), and the conversion between the Ag/AgCl and RHE was performed using the equation:

$$E_{\text{RHE}} = E_{\text{Ag/AgCl}} + 0.059 \text{ pH} + 0.197 \text{ V}$$

Incident photon-to-current efficiency (IPCE) at each wavelength was determined using illumination from a 300 W Xe arc lamp and neutral density filters, to imitate the light from the sun. Monochromatic light was produced using an Oriel Cornerstone 130 monochromator with a 10 nm bandpass, and the output was measured using a photodiode detector. IPCE was measured at 0.6 V vs. RHE using the same three-electrode setup described above for the photocurrent measurements.

$$\text{IPCE} = \frac{J \times \lambda}{P_{\text{light}}} \times 100\%$$

where: *J* is the photocurrent density, *λ* is the incident light wavelength and *P*<sub>light</sub> is the measured irradiance.

The applied bias photon-to-current efficiency (ABPE) was calculated from a *J*-*V* curve, where: *J* is the photocurrent density,



$V_{\text{bias}}$  is the applied bias and  $P_{\text{in}}$  is the incident illumination power density ( $\text{AM } 1.5 \text{ G}, 100 \text{ mW cm}^{-2}$ ):

$$\text{ABPE} = \frac{J \times (1.23 - V_{\text{bias}})}{P_{\text{in}}} \times 100\%$$

The  $\eta_{\text{tr}}$  was calculated using the equation:

$$\eta_{\text{tr}} = J_{\text{water}}/J_{\text{Na}_2\text{SO}_3}$$

where:  $J_{\text{water}}$  is the  $\text{TiO}_2/\text{BiVO}_4$  electrode photocurrent density in 0.1 M PBS,  $J_{\text{Na}_2\text{SO}_3}$  is the  $\text{TiO}_2/\text{BiVO}_4$  electrode photocurrent density in 0.1 M PBS containing 0.1 M  $\text{Na}_2\text{SO}_3$ .

## Results and discussion

A porous  $\text{BiVO}_4$  was produced using the previously reported method.<sup>10</sup> Fig. 1a shows the microstructure of the porous  $\text{BiVO}_4$ ; the significant voids can be seen clearly. The porous structure of the  $\text{BiVO}_4$  enables sites for the  $\text{TiO}_2$  nanospheres to attach.  $\text{TiO}_2$  nanospheres, with a range of diameter size 200 to 500 nm (illustrated by DLS in Fig S3<sup>†</sup>) were attached onto the  $\text{BiVO}_4$  electrodes using a hydrothermal method. The SEMs of  $\text{TiO}_2/\text{BiVO}_4$  electrodes with different hydrothermal times are shown in Fig. 1b–d, which show that the  $\text{TiO}_2$  nanospheres were attached onto the  $\text{BiVO}_4$  successfully and the quantity of  $\text{TiO}_2$  nanospheres increased with immersed time. The elemental mapping results shown in Fig. 1e–h suggest the existence of O, Ti, Bi, and V elements, indicating a uniform distribution of  $\text{TiO}_2$  nanospheres across the structure.

The crystalline structures of the FTO,  $\text{BiVO}_4$  and  $\text{TiO}_2/\text{BiVO}_4$  samples were characterised using X-ray diffraction (XRD) patterns, as shown in Fig S4,<sup>†</sup> further confirming that  $\text{TiO}_2$  attached to the porous  $\text{BiVO}_4$  and that the crystalline structures of  $\text{TiO}_2$  are anatase.

In order to gain more insight into  $\text{TiO}_2/\text{BiVO}_4$  heterojunctions, X-ray photoelectron spectroscopy (XPS) characterisation was performed, which showed signals from Ti, O, Bi

and V elements (Fig. S5<sup>†</sup>). The HR-XPS spectra of the  $\text{TiO}_2/\text{BiVO}_4$  are shown in Fig. 2. Two binding energy peaks for a typical Bi element in  $\text{BiVO}_4$  occurred at 158.9 and 164.2 eV, corresponding to the Bi 4f7/2 and Bi 4f5/2, suggesting that Bi is present as  $\text{Bi}^{3+}$  (Fig. 2a).<sup>34</sup> The binding energies of the vanadium(v) peaks were centred at 516.5 and 524.5 eV, corresponding to V 2p3/2 and V 2p1/2 orbits, respectively, characteristic of the presence of the  $\text{V}^{5+}$  oxidation state (Fig. 2b).<sup>35</sup> Two peaks for Ti 2p at 458.7 and 465.7 eV were assigned to Ti 2p3/2 and Ti 2p1/2, respectively, suggesting a  $\text{Ti}^{4+}$  oxidation state (Fig. 2c).<sup>36</sup> The peak at binding energy of 529.8 eV in Fig. 2d, indicates that oxygen was present as surface lattice oxygen and free oxygen.<sup>37</sup>

The PEC performance of the  $\text{BiVO}_4$  and  $\text{TiO}_2/\text{BiVO}_4$  was measured using a three electrode system which included the proposed electrode as the working electrode, an Ag/AgCl (3.5 M KCl) reference and a platinum counter electrode. Fig. 3a shows the linear sweep voltammetry (LSV) curves of the  $\text{BiVO}_4$  and  $\text{TiO}_2/\text{BiVO}_4$  electrodes. In the dark those electrodes show little photocurrent density. However, in the light, the differences in the  $\text{TiO}_2$  on the  $\text{BiVO}_4$  electrode resulted in a different photocurrent density, and  $\text{TiO}_2/\text{BiVO}_4$  electrodes had a significantly enhanced photocurrent density compared to  $\text{BiVO}_4$  and  $\text{TiO}_2$  electrodes. The 30 min- $\text{TiO}_2/\text{BiVO}_4$  electrode had the highest photocurrent density, with a value of  $3.3 \text{ mA cm}^{-2}$  at 1.23 V vs. RHE, which was 2.5 times that of  $\text{BiVO}_4$ . However, the 60 min- $\text{TiO}_2/\text{BiVO}_4$  electrode had lower photocurrent density compared to 30 min- $\text{TiO}_2/\text{BiVO}_4$ , which may be a result of  $\text{TiO}_2$  hindering charge transfer. A significant cathodic shift of onset potential was observed. For the 30 min- $\text{TiO}_2/\text{BiVO}_4$  electrode, the potential at  $0.5 \text{ mA cm}^{-2}$  was reduced greater than 500 mV, indicating an efficient charge separation or charge transfer originating from the formation of a heterojunction.

To test the charge recombination behaviour of the  $\text{TiO}_2/\text{BiVO}_4$  electrodes, 0.1 M  $\text{Na}_2\text{SO}_3$  solution was added to the electrolyte as a hole scavenger for the PEC measurements. The LSV curves of  $\text{TiO}_2/\text{BiVO}_4$  electrodes are shown in Fig. 3b.  $\text{TiO}_2/$

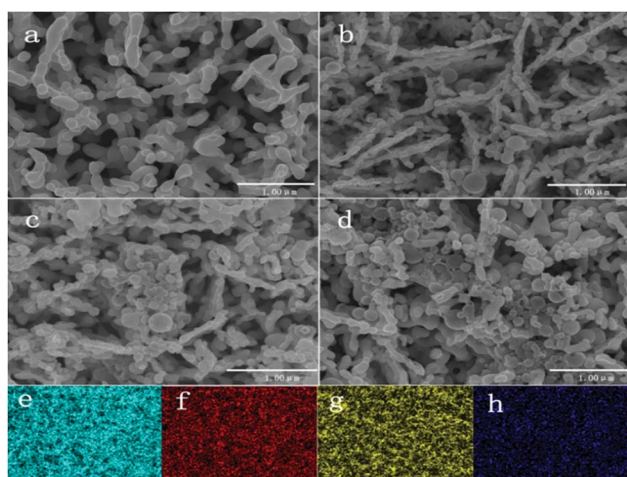


Fig. 1 SEMs of different electrodes. (a)  $\text{BiVO}_4$ , (b) 10 min- $\text{TiO}_2/\text{BiVO}_4$ , (c) 30 min- $\text{TiO}_2/\text{BiVO}_4$ , (d) 60 min- $\text{TiO}_2/\text{BiVO}_4$ , and EDX-mapping of  $\text{TiO}_2/\text{BiVO}_4$  are shown (e) Bi, (f) V, (g) O, (h) Ti.

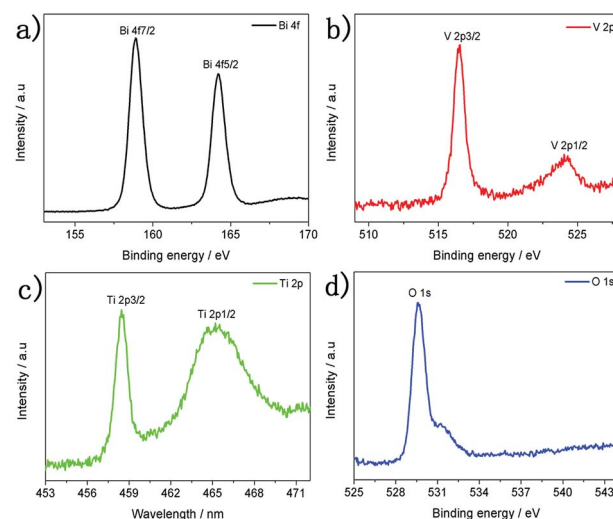
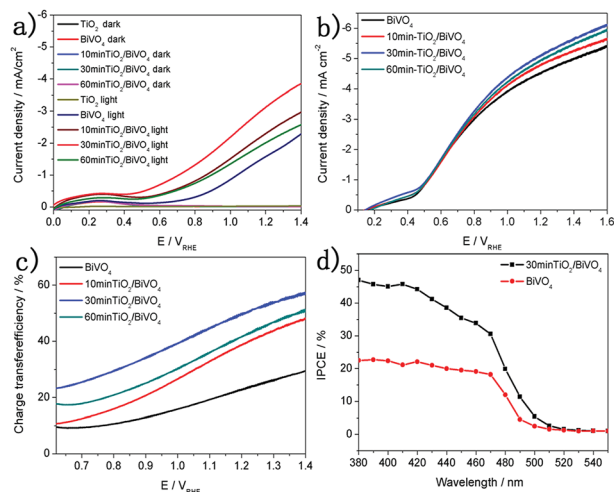


Fig. 2 XPS spectra of the  $\text{TiO}_2/\text{BiVO}_4$  electrode (a) Bi 4f, (b) V 2p, (c) Ti 2p, (d) O 1s.







**Fig. 3** (a) LSV curves of different  $\text{TiO}_2/\text{BiVO}_4$  electrodes. (b) LSV of curves  $\text{BiVO}_4$  and  $\text{TiO}_2/\text{BiVO}_4$  in 0.1 M PBS containing 0.1 M  $\text{Na}_2\text{SO}_3$ . (c) The charge transfer efficiencies of different  $\text{TiO}_2$  content on  $\text{BiVO}_4$ . (d) IPCEs of  $\text{BiVO}_4$  and  $\text{TiO}_2/\text{BiVO}_4$  electrodes.

$\text{BiVO}_4$  electrodes show higher photocurrent density compared to the  $\text{BiVO}_4$  electrode, demonstrating a heterojunction was formed and better charge separation occurred. The 30 min- $\text{TiO}_2/\text{BiVO}_4$  electrode had the highest photocurrent density,  $5.4 \text{ mA cm}^{-2}$  at 1.23 V vs. RHE. The photocurrent can be described as:  $J = J_{\text{abs}} \times \eta_{\text{sep}} \times \eta_{\text{tr}}$ <sup>38</sup> the  $\eta_{\text{tr}}$  values can be calculated as  $J_{\text{water}}/J_{\text{Na}_2\text{SO}_3}$ . As shown in Fig. 3c, all  $\text{TiO}_2/\text{BiVO}_4$  electrodes had improved  $\eta_{\text{tr}}$  compared to the  $\text{BiVO}_4$  electrode, over the range tested in this study. The 30 min- $\text{TiO}_2/\text{BiVO}_4$  electrode had the highest  $\eta_{\text{tr}}$ , 60% at 1.23 V vs. RHE, 3 times that of the  $\text{BiVO}_4$  electrode. These results demonstrate that the construction of a  $\text{TiO}_2/\text{BiVO}_4$  heterojunction could promote charge separation and charge transfer efficiencies. The incident-photon-to-current-conversion efficiency (IPCE) values are shown in Fig. 3d. The  $\text{TiO}_2/\text{BiVO}_4$  was higher than  $\text{BiVO}_4$  across the visible spectrum and at 520 nm the two electrodes reached 0, which is in agreement with the light absorbance of  $\text{BiVO}_4$  and  $\text{TiO}_2/\text{BiVO}_4$  electrodes (Fig S6<sup>†</sup>).

The photocurrent transient behaviours of the  $\text{TiO}_2/\text{BiVO}_4$  electrodes were measured in 0.1 M PBS. A photocurrent spike was obtained using sudden illumination due to capacitive charging of the interface, and the spike decay due to the recombination of the electrons and holes that is associated with holes getting trapped at the electrode surface. A stabilised photocurrent was achieved when the charge generation and recombination rates were equal. Furthermore, the recombination rate could be reflected by longer transient decay times, which can be analysed on a logarithmic plot of parameter  $D$ , using the following equation:<sup>39</sup>

$$D = (I_t - I_s)/(I_m - I_s)$$

where:  $I_t$  is the photocurrent density at time  $t$ ,  $I_s$  is the stabilised photocurrent density and  $I_m$  is the photocurrent density spike. The transient decay time can be defined as the time at which  $\ln D = -1$ . Fig. 4a shows the logarithmic plots of parameter  $D$  of

the  $\text{BiVO}_4$  and  $\text{TiO}_2/\text{BiVO}_4$  electrodes. The transient decay time for  $\text{TiO}_2/\text{BiVO}_4$  was 4.1 s, longer than that of  $\text{BiVO}_4$  (1.5 s), suggesting a lower rate of electron and hole recombination in  $\text{TiO}_2/\text{BiVO}_4$ , which could be attributed to the  $\text{TiO}_2$  nanospheres acting as hole resistors, resulting in increased efficiency of charge separation and prolonging the lifetime of the holes. As a result, abundant photogenerated charge carriers in the  $\text{TiO}_2/\text{BiVO}_4$  electrode were effectively collected, leading to an improved PEC performance.

To characterise the kinetics of the charge transfer process of the  $\text{TiO}_2/\text{BiVO}_4$  and  $\text{BiVO}_4$  electrodes, electrochemical impedance spectroscopy (EIS) tests were performed at 1.23 V vs. RHE in 0.1 M PBS under simulated solar light illumination. Fig. 4b shows Nyquist at frequencies from 1 Hz to 100 kHz. The  $\text{BiVO}_4$  electrode had the greatest resistance to charge transfer and the 30 min- $\text{TiO}_2/\text{BiVO}_4$  had the lowest charge transfer resistance. However, the 60 min- $\text{TiO}_2/\text{BiVO}_4$  electrode had a lower charge transfer resistance, which may be a result of the  $\text{TiO}_2$  impeding the transfer of surface charge, further indicating the optimum amount of  $\text{TiO}_2$  was achieved in the 30 min- $\text{TiO}_2/\text{BiVO}_4$  electrode. The above results suggest that the  $\text{TiO}_2$  facilitates the  $\text{BiVO}_4$  electrode charge separation and transfer.

In order to further investigate the PEC performance, a molecular Co-cubane water oxidation catalyst was immobilised onto the  $\text{TiO}_2/\text{BiVO}_4$  electrode. As the LSV curves show in Fig. 5a, the Co-cubane/ $\text{TiO}_2/\text{BiVO}_4$  photoanode exhibits a high photocurrent density of  $4.6 \text{ mA cm}^{-2}$  at 1.23 V vs. RHE, 3.1 times higher than that of  $\text{BiVO}_4$ , indicating that the Co-cubane was acting as an efficient OER catalyst, further enhancing the charge transfer. Furthermore, after 400 s photoelectrolysis, the photocurrent density of Co-cubane/ $\text{TiO}_2/\text{BiVO}_4$  could maintain more than  $2.6 \text{ mA cm}^{-2}$ , which is 2.6 times than that of the bare  $\text{BiVO}_4$  (Fig S7<sup>†</sup>). The half-cell photoconversion efficiencies of  $\text{BiVO}_4$  and Co-cubane/ $\text{TiO}_2/\text{BiVO}_4$  electrodes were calculated using the LSV results, (Fig. 5b). The maximum value of Co-cubane/ $\text{TiO}_2/\text{BiVO}_4$  achieved 1.48% at 0.72 V, approximately 6 fold compared to  $\text{BiVO}_4$ . The XPS spectra of the Co-cubane/ $\text{TiO}_2/\text{BiVO}_4$  electrode was shown in Fig S8,† which indicated the element of Co was exited.

To explore the charge transfer mechanism between the  $\text{BiVO}_4$  and  $\text{TiO}_2$ , Mott-Schottky plots of the  $\text{BiVO}_4$  and  $\text{TiO}_2$  were performed under dark conditions.<sup>40</sup> In Fig S9b,† the linear part of Mott-Schottky plots of  $\text{TiO}_2/\text{BiVO}_4$  rather than  $\text{BiVO}_4$  show the gentlest slope and the more negative flatband potential. The gentle slope means the modifying with  $\text{TiO}_2$  can obviously

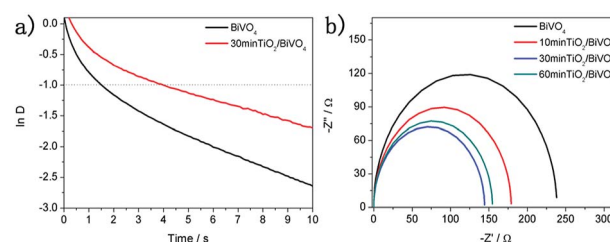


**Fig. 4** (a) The logarithmic plots of the parameter  $D$  of the  $\text{BiVO}_4$  and  $\text{TiO}_2/\text{BiVO}_4$  electrodes. (b) Electrochemical impedance spectroscopy (EIS) of the  $\text{TiO}_2$  under different soaking times.



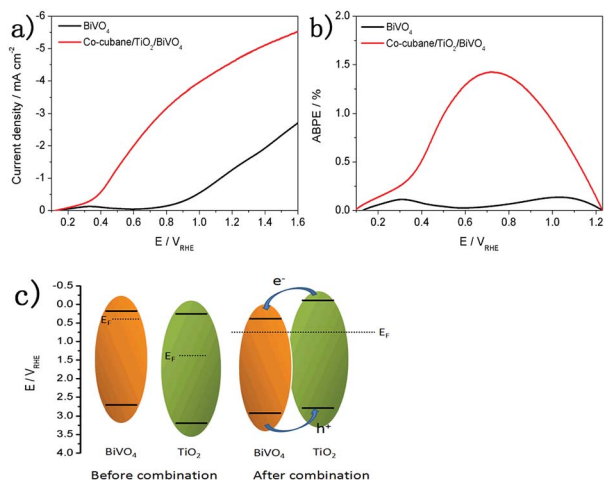


Fig. 5 (a) LSV curves of  $\text{BiVO}_4$  and Co-cubane/ $\text{TiO}_2/\text{BiVO}_4$  electrodes. (b) ABPEs of  $\text{BiVO}_4$  and Co-cubane/ $\text{TiO}_2/\text{BiVO}_4$  electrodes. (c) The charge transfer mechanism of  $\text{TiO}_2/\text{BiVO}_4$  electrode.

increase the density of the carriers.<sup>41</sup> From Fig S9a and c,<sup>†</sup> the CB position of  $\text{BiVO}_4$  and  $\text{TiO}_2$  were 0.12 eV and 0.2 eV. And from Fig S10,<sup>†</sup> the band gap energies of  $\text{BiVO}_4$  and  $\text{TiO}_2$  were 2.42 eV and 3.09 eV. Therefore, the VB position of  $\text{BiVO}_4$  and  $\text{TiO}_2$  were 2.54 eV and 3.29 eV, calculated using  $E_{\text{CB}} = E_{\text{VB}} - E_{\text{g}}$ . Compared the  $\text{BiVO}_4$ , the  $\text{TiO}_2$  approach to the intrinsic semiconductor. So we suppose the charge transfer mechanism shown the Fig. 5c, When these two types of semiconductor materials are closely joined together, the heterojunction structure was formed. At this moment, the two semiconductors have a uniform Fermi level and the system is in equilibrium. An electron transfer from  $\text{TiO}_2$  to  $\text{BiVO}_4$  possibly occurred, providing evidence for the efficient charge transfer between  $\text{BiVO}_4$  and  $\text{TiO}_2$ .

## Conclusions

In summary, a simple hydrothermal method was proposed to produce a  $\text{TiO}_2/\text{BiVO}_4$  heterojunction electrode. The proposed  $\text{TiO}_2/\text{BiVO}_4$  electrode provided a high performance for the oxidation of PEC water. The  $\text{TiO}_2/\text{BiVO}_4$  heterojunction results indicate good charge separation and transfer efficiency. When a molecular Co-cubane catalyst was attached onto the  $\text{TiO}_2/\text{BiVO}_4$  electrode, a further improvement in the PEC performance was achieved, with a photocurrent density of photocurrent density of  $4.6 \text{ mA cm}^{-2}$  at 1.23 V, more than 3 times for  $\text{BiVO}_4$  alone. This study provides a simple and effective approach in the production of heterojunction photoelectrodes for increasing the performance of PEC, which could be used to design efficient photocatalytic systems in future studies.

## Conflicts of interest

The authors declare no conflict of interest.

## Acknowledgements

This work was supported by the National Natural Science Foundation of China (21401092, 21671089, 21773100), the Shenyang Natural Science Foundation of China (F16-103-4-00), Scientific Research Found of Liaoning Province (LT2017010, 20170540409, 20180510011).

## References

- 1 A. Kudo and Y. Miseki, *Chem. Soc. Rev.*, 2009, **38**, 253–278.
- 2 O. Khaselev, *Science*, 1998, **280**, 425–427.
- 3 Z. Li, W. Luo, M. Zhang, J. Feng and Z. Zou, *Energy Environ. Sci.*, 2013, **6**, 347–370.
- 4 M. Grätzel, *Nature*, 2001, **414**, 338–344.
- 5 K. O. Akihiko Kudo and H. Kato, *J. Am. Chem. Soc.*, 1999, **121**, 11459–11467.
- 6 F. E. Osterloh, *Chem. Soc. Rev.*, 2013, **42**, 2294–2320.
- 7 Z. Yin, Z. Wang, Y. Du, X. Qi, Y. Huang, C. Xue and H. Zhang, *Adv. Mater.*, 2012, **24**, 5374–5378.
- 8 H. K. Saimi Tokunaga and A. Kudo, *Chem. Mater.*, 2001, **13**, 4624–4628.
- 9 M. Zhong, T. Hisatomi, T. Minegishi, H. Nishiyama, M. Katayama, T. Yamada and K. Domen, *J. Mater. Chem. A*, 2016, **4**, 9858–9864.
- 10 T. W. Kim and K. S. Choi, *Science*, 2014, **343**, 990–994.
- 11 G. Wang, Y. Ling, X. Lu, F. Qian, Y. Tong, J. Z. Zhang, V. Lordi, C. Rocha Leao and Y. Li, *J. Phys. Chem. C*, 2013, **117**, 10957–10964.
- 12 Y. Park, D. Kang and K. S. Choi, *Phys. Chem. Chem. Phys.*, 2014, **16**, 1238–1246.
- 13 M. Huang, J. Bian, W. Xiong, C. Huang and R. Zhang, *J. Mater. Chem. A*, 2018, **6**, 3602–3609.
- 14 B. Klahr, S. Gimenez, F. Fabregat-Santiago, J. Bisquert and T. W. Hamann, *J. Am. Chem. Soc.*, 2012, **134**, 16693–16700.
- 15 C. Zachus, F. F. Abdi, L. M. Peter and R. van de Krol, *Chem. Sci.*, 2017, **8**, 3712–3719.
- 16 F. F. Abdi and R. van de Krol, *J. Phys. Chem. C*, 2012, **116**, 9398–9404.
- 17 B. Zhang, L. Wang, Y. Zhang, Y. Ding and Y. Bi, *Angew. Chem., Int. Ed. Engl.*, 2018, **57**, 2248–2252.
- 18 H. Zhang, Y. Yu, L. Zhang and S. Dong, *Angew. Chem., Int. Ed. Engl.*, 2018, **57**, 1547–1551.
- 19 S. Gu, W. Li, F. Wang, S. Wang, H. Zhou and H. Li, *Appl. Catal., B*, 2015, **170–171**, 186–194.
- 20 A. P. Singh, N. Kodan, B. R. Mehta, A. Held, L. Mayrhofer and M. Moseler, *ACS Catal.*, 2016, **6**, 5311–5318.
- 21 S.-W. Cao, Z. Yin, J. Barber, F. Y. C. Boey, S. C. J. Loo and C. Xue, *ACS Appl. Mater. Interfaces*, 2011, **4**, 418–423.
- 22 L. Zhang, L. O. Herrmann and J. J. Baumberg, *Sci. Rep.*, 2015, **5**, 16660.
- 23 H. Hirakawa, S. Shiota, Y. Shiraiishi, H. Sakamoto, S. Ichikawa and T. Hirai, *ACS Catal.*, 2016, **6**, 4976–4982.
- 24 J. Su, L. Guo, N. Bao and C. A. Grimes, *Nano Lett.*, 2011, **11**, 1928–1933.
- 25 P. Chatchai, Y. Murakami, S.-y. Kishioka, A. Y. Nosaka and Y. Nosaka, *Electrochim. Acta*, 2009, **54**, 1147–1152.



- 26 Y. Pihosh, I. Turkeyvych, K. Mawatari, T. Asai, T. Hisatomi, J. Uemura, M. Tosa, K. Shimamura, J. Kubota, K. Domen and T. Kitamori, *Small*, 2014, **10**, 3692–3699.
- 27 S. Ho-Kimura, S. J. A. Moniz, A. D. Handoko and J. Tang, *J. Mater. Chem. A*, 2014, **2**, 3948–3953.
- 28 H. Zhang and C. Cheng, *ACS Energy Lett.*, 2017, **2**, 813–821.
- 29 M. Xie, X. Fu, L. Jing, P. Luan, Y. Feng and H. Fu, *Adv. Energy Mater.*, 2014, **4**, 1300995.
- 30 J. S. Yang, W. P. Liao and J. J. Wu, *ACS Appl. Mater. Interfaces*, 2013, **5**, 7425–7431.
- 31 Y. Ma, X. Wang, Y. Jia, X. Chen, H. Han and C. Li, *Chem. Rev.*, 2014, **114**, 9987–10043.
- 32 D. Lee, A. Kvit and K.-S. Choi, *Chem. Mater.*, 2018, **30**, 4704–4712.
- 33 S. S. Kalanur, I.-H. Yoo, J. Park and H. Seo, *J. Mater. Chem. A*, 2017, **5**, 1455–1461.
- 34 L. Dong, S. Guo, S. Zhu, D. Xu, L. Zhang, M. Huo and X. Yang, *Catal. Commun.*, 2011, **16**, 250–254.
- 35 Y. Guo, X. Yang, F. Ma, K. Li, L. Xu, X. Yuan and Y. Guo, *Appl. Surf. Sci.*, 2010, **256**, 2215–2222.
- 36 N. Myung, S. Ham, S. Choi, Y. Chae, W.-G. Kim, Y. J. Jeon, K.-J. Paeng, W. Chanmanee, N. R. de Tacconi and K. Rajeshwar, *J. Phys. Chem. C*, 2011, **115**, 7793–7800.
- 37 N. J. Bell, Y. H. Ng, A. Du, H. Coster, S. C. Smith and R. Amal, *J. Phys. Chem. C*, 2011, **115**, 6004–6009.
- 38 D. K. Zhong, S. Choi and D. R. Gamelin, *J. Am. Chem. Soc.*, 2011, **133**, 18370–18377.
- 39 A. L. Hagfeldt, H. Lindström, S. Soedergrén and S.-E. Lindquist, *J. Electroanal. Chem.*, 1995, **381**, 39–46.
- 40 J. A. T. G. Cooper and A. J. Nozik, *J. Electrochem. Soc.*, 1982, **129**, 1973–1977.
- 41 F. Ning, M. Shao, S. Xu, Y. Fu, R. Zhang, M. Wei, D. G. Evans and X. Duan, *Energy Environ. Sci.*, 2016, **9**, 2633.

